Title
Cardiothoracic Applications of 3-dimensional Printing

Permalink
https://escholarship.org/uc/item/0fn7066d

Authors
Giannopoulos, Andreas A
Steigner, Michael L
George, Elizabeth
et al.

Peer reviewed

Cardiothoracic Applications of 3D Printing

Andreas A. Giannopoulos[1], **Michael L. Steigner**[1], **Elizabeth George**[1], **Maria Barile**[2], **Andetta R. Hunsaker**[2], **Frank J. Rybicki**[3], and **Dimitris Mitsouras**[1]

[1]Applied Imaging Science Laboratory, Brigham and Women's Hospital, Boston, MA, USA

[2]Division of Thoracic Imaging, Radiology Department, Brigham and Women's Hospital, Boston, MA, USA

[3]Department of Radiology, The University of Ottawa Faculty of Medicine and The Ottawa Hospital Research Institute, Ottawa, ON, Canada

Summary

Medical 3D printing is emerging as a clinically relevant imaging tool in directing preoperative and intraoperative planning in many surgical specialties and will therefore likely lead to interdisciplinary collaboration between engineers, radiologists, and surgeons. Data from standard imaging modalities such as CT, MRI, echocardiography and rotational angiography can be used to fabricate life-sized models of human anatomy and pathology, as well as patient-specific implants and surgical guides. Cardiovascular 3D printed models can improve diagnosis and allow for advanced pre-operative planning. The majority of applications reported involve congenital heart diseases, valvular and great vessels pathologies. Printed models are suitable for planning both surgical and minimally invasive procedures. Added value has been reported toward improving outcomes, minimizing peri-operative risk, and developing new procedures such as transcatheter mitral valve replacements. Similarly, thoracic surgeons are using 3D printing to assess invasion of vital structures by tumors and to assist in diagnosis and treatment of upper and lower airway diseases. Anatomic models enable surgeons to assimilate information more quickly than image review, choose the optimal surgical approach, and achieve surgery in a shorter time. Patient-specific 3D-printed implants are beginning to appear and may have significant impact on cosmetic and life-saving procedures in the future. In summary, cardiothoracic 3D printing is rapidly evolving and may be a potential game-changer for surgeons. The imager who is equipped with the tools to apply this new imaging science to cardiothoracic care is thus ideally positioned to innovate in this new emerging imaging modality.

Keywords

three-dimensional printing; 3D printing; cardiovascular applications; thoracic applications; cardiothoracic imaging

Address correspondence to: Dimitrios Mitsouras, PhD, Brigham and Women's Hospital, Harvard Medical School, 75 Francis Street, Boston, MA 02115, Tel +1.617.732.7206, Fax +1.617.264.5232, dmitsouras@partners.org.

Introduction

Three-dimensional (3D) printing enables the conversion of images from medical imaging modalities including Computed Tomography (CT), Magnetic Resonance (MR), and even 3-dimensional (3D) ultrasound (US) into hand-held models that can be quickly inspected, understood, and manipulated in a surgical setting. The utility of these models for planning and simulating surgical procedures, identifying anatomic landmarks, potential vascular and other vital organ involvement, with attendant complications carries a high degree of usefulness to many surgical specialties including thoracic and cardiac surgery. As with the development of any new medical technology, early research efforts in 3D printing [1–3] and subsequent clinical case reports [4–9] are now being followed by a growing number of studies with concrete outcomes to establish its utility in various clinical settings [10–15], not only for preoperative planning and simulation, but also in the construction of patient-specific implants and in physician training [16–18].

The versatility of 3D printing in conjunction with the complexity of developing a clinically useful model that conveys pathology efficiently and effectively will likely lead to 3D printing being considered a distinct imaging modality in the future. Radiologists are poised to direct and facilitate its integration into medical practice [19]. At present, cardiothoracic imagers are spearheading this effort as cardiothoracic models comprise the second most-reported application of 3D printing, following musculoskeletal and cranio-maxillofacial models. The anatomic complexity and diversity of imaging techniques involved in cardiothoracic imaging certainly renders 3D printing more challenging than in other applications [19]. This review familiarizes the reader with 3D printing and its applications in cardiac and thoracic imaging. A review of case reports, technical notes and clinical studies over the last 15 years (2000–2015), organized in a per-organ fashion will serve as a guide to indications that the reader can refer to as they begin to integrate 3D printing in their own practice. To this end, specific imaging modalities and printing technologies are discussed, as are recent advances that readers can contribute to with their own research.

The Methods of 3D Printing Medical Images

Imaging

The first step for 3D printing involves the acquisition of thin-section image data (ideally 0.75 to 1 mm) which are then reconstructed into a 3D (volumetric) dataset. Excellent tissue contrast between the tissues of interest is required as a 3D-printed model cannot convey information regarding tissues that are either not visualized in the imaging modality used to acquire the source images or that do not have sufficient differences in image intensity/signal characteristics from adjacent tissues. For example, nerves are not clearly delineated on a standard CT, thus it would not be possible to create a 3D model demonstrating the relationship of the brachial plexus to a superior sulcus tumor from CT. It is however possible to fuse multiple imaging modalities to create such a model, for example, the bone and vasculature can be visualized in a contrast enhanced CT and the nerves on an MRI of the brachial plexus. A single 3D-printed model showing the tissues seen in each examination independently can be created during the following two steps of the 3D printing process.

Tissue Segmentation

The second step involves carefully segmenting each tissue on the source images so as to demarcate its boundaries from those of adjacent tissues. One typically segments only those tissues that are relevant to the proposed surgical procedure. For example in a case of chest wall tumor, the adjacent portion of the ribcage and the vascular supply may be deemed pertinent to print in addition to the tumor itself, but not the mediastinal structures which are outside the surgical field. This is necessary not only because segmentation is a time-consuming and (currently) manually laborious task, but also because the efficacy and thus clinical utility of the model hinges on its ability to quickly communicate the relevant information. Thus, while an anterior mediastinal mass model could contain the entire ribcage and thoracic spine, the resulting model would likely present difficulties in clearly visualizing the tumor and in aiding comprehension of its relationship to more crucial mediastinal structures. In this context, 3D printing of complex cardiothoracic models at present also demands an artistic component to select the relevant tissues and enable their optimal visualization. The latter subject is further discussed below (see Computer-Aided Design section below). Future research should aim to establish guidelines as to what tissues are useful to include in a model for each specific indication.

STL Model Generation

Tissues that have been segmented by demarcating their boundaries in the individual, successive 2D cross-sectional images that compose the 3D image volume cannot be directly 3D-printed. A third step is required to assemble a model of those tissues that a 3D printer can interpret. This model is a closed surface that fully encloses all the voxels segmented to belong to a single structure to be printed. The most common format for this surface model is a mesh composed of triangles and stored as a standard tessellation language (STL; also referred to as a stereolithography) file format (Figure 1). The STL file format is thus to 3D printers what the Digital Imaging and Communications in Medicine (DICOM) format is to radiology workstations. Workstation software knows how to interpret the image intensities stored in DICOM files so as to display them as an image on a monitor. Similarly, 3D printer drivers know how to interpret the triangles in an STL file so as to manufacture the object enclosed by them. The above three steps has often been collectively referred to as converting DICOM images into an STL file format.

Computer-Aided Design STL Manipulations

A fourth step that is new to radiologists is often required to produce a clinically-useful 3D printed model. This step involves manipulating and augmenting the STL representations of the segmented tissues using computer-aided design (CAD) software to exemplify the pathology and maximize the surgical utility of the model. Some of these manipulations are used in almost every 3D-printed cardiothoracic model. One example shown in Figure 2 is the addition of connectors such as cylinders between separate anatomical structures of interest, for example the clavicle and ribs in a model that does not need to include the sternum. The connectors enable these separate structures to stay together and maintain their spatial position when printed. Two CAD manipulations that are similarly common for cardiovascular model creation are shown in Figure 3. The first is that of generating a hollow

model of the lumen of an artery or vein for which the blood pool has been segmented from a contrast enhanced angiogram. The hollow model can be used to e.g., simulate a catheter angiography procedure [20]. The second is the design of cutout windows such as in a vessel wall or myocardium so as to allow the interventionalist to easily inspect the pathology (e.g., a mural thrombus in Figure 3). Cutout windows can be included in the model as removable parts, enabling visualization of the entire organ when in place. This also requires CAD tools to introduce appropriate snap-fit connectors to keep those components in place (Figure 3).

Many more complex STL manipulations are used to achieve or simplify the creation of a model. A final important manipulation for cardiothoracic models is the "shrink-wrapping" operation which closes small gaps in an STL model. This can be useful in thoracic models when high resolution CT images visualize the articulations of the ribs with the vertebrae. Automated segmentation based on bone density is likely to result in ribs unattached to the vertebrae. While connectors can be manually introduced in the joint spaces with significant labor, the shrink-wrapping operation can close these small spaces automatically, enabling an attached model to be printed. In cardiovascular models, shrink-wrapping is useful for example to produce the hypothetical vessel wall in the presence of filling defects such as for example due to mural thrombi in the aorta in Figure 3. Finally, STL CAD manipulations are required for the creation of patient-specific implants. For example, if one is developing a custom-made prosthesis for chest wall reconstruction, it must be computationally designed using CAD tools to ideally fit the contour of the STL of the patient's thoracic cavity as visualized in pre-operative imaging.

Radiologist involvement is crucial for the generation and post-processing of STL models as inaccuracies are easily introduced and to date there have been no published guidelines, nor are there standardized methods readily available. For example, operations such as wrapping and smoothing can simplify the creation of a model but may change its dimensions and thus impact device sizing using the model that could otherwise be avoided by radiologist's measurements on the source images and 3D renderings. Trial and error, by superposition of the modified STL models onto the source images (see e.g., Figure 3), as well as building proficiency and standardizing one's methodology are common practice amongst early adopters of this technology. Even with experience, generating printable STLs is a lengthy process. The average time for the creation of a model including segmentation, STL generation and CAD manipulations in our lab varies from 2 to 20 hours, depending on the complexity of the pathology and intended use of the model. Using available commercial software platforms, creating a model of the blood pool for example will require little time for segmentation and STL generation, and may even require no CAD manipulations. A model of the vessel wall that can be used to plan an endovascular procedure and that demonstrates distinct atherosclerotic plaques (Figure 3) on the other hand may require 8 hours of CAD manipulations, including trial and error to achieve an optimal result.

A number of commercial and free software packages are available to perform each of the above steps. The most comprehensive medical 3D printing software is the Mimics suite (Materialise, Leuven, Belgium) which includes the most extensive set of segmentation and CAD tools. In terms of separate components, Vitrea (Vital Images Inc, Minnetonka, MN) for example provides tools familiar to radiologists for segmentation and STL file generation,

while OsiriX (Pixmeo, Geneva, Switzerland) offers a free alternative for those steps. CAD tools necessary to couple with these softwares include 3-matic (Materialise, Leuven, Belgium), AutoCAD (Autodesk Inc, San Rafael, CA), or the freely-available Meshmixer (Autodesk Inc, San Rafael, CA). In our lab we primarily use Mimics, or the combination of Vitrea and 3-matic whenever automated segmentation protocols in the former suffice to generate an STL suitable for 3D printing.

3D Printing Technologies

Models stored in STL files are printed using a 3D printer. A variety of 3D printing technologies are available that can print in diverse materials from plastics to metals. In summary, four distinct 3D printing technologies are mainly used to produce anatomic models, namely material jetting, stereolithography (SLA), fused deposition modeling (FDM), and binder jetting. One technology, powder bed fusion, is instead mainly used to print implants and prostheses. Two examples of this latter technology encountered in the medical literature are selective laser sintering (SLS) and electron beam melting (EBM). More details are provided below for those technologies most commonly encountered in the literature.

Anatomic Models and Biocompatible Surgical Guides

Material jetting and SLA both print using photopolymers such as acrylics that can be rigid or flexible, and transparent or opaque. Short-term biocompatible materials (up to 30 days) are available for printing e.g., surgical guides. SLA produces a smooth finish but is limited to single-color single-material prints. Material jetting can print multiple colors and material properties in a single model, with slightly rougher finish. FDM is a lower resolution printing modality that typically prints using thermoplastics. It has limited capacity to use multiple colors and materials in a single print, and printed models tend to have rough surface finish. Finally, binder jetting can print vibrant multi-color models using typically gypsum powder. Models are fragile and with granular surface finish, but can have a lacquered finish and be flexible after infiltration with acrylics and elastomers.

In our experience, the most versatile printing technology for medical models is material jetting. Similar to an inkjet printer, it instead jets a photoreactive liquid containing monomers and oligomers that cross-link to form polymers (photopolymers) once exposed to typically ultraviolet (UV) light. The printer heads scan across the build tray jetting photopolymer at the locations occupied by the object to be printed at each successive layer, and a UV lamp initiates their polymerization. This technology uniquely offers extensive freedom to produce multi-material in addition to multi-color 3D-printed models, as photopolymers can be mixed during jetting. For example, a rigid and a flexible photopolymer can be combined to print a model with flexible material for soft tissues, hard material for a calcification or bone, and material of an intermediate hardness for e.g., a surgical adhesion. This feature renders this technology the most commonly-used in cardiovascular applications. However, printers are expensive ($30,000 for single material to several hundred thousand for multi-material). SLA uses the same chemistry as material jetting, but is limited to single-material printing as the photopolymer is held in a vat. A UV

light source (typically a laser) traces the object cross-section at the surface of the liquid, just under which sits the build tray. The build tray is either submersed by one layer thickness into the vat (top-to-bottom printers) or lifted by one layer thickness from a transparent-floored vat (bottom-up printers) through which the laser shines to print the next layer. Consumer SLA printers are available for <$5,000, although large printers have a similar price range as material jetting systems. Print resolution for both material jetting and SLA are as high as 30 μm, and small features of the order of 300 μm can be printed.

FDM is also important as it is currently the most often-encountered technology in the medical 3D printing research literature, likely given the low price of consumer-grade printers (<$1,000–5,000). A filament of thermoplastic material such as acrylonitrile butadiene acrylate (ABS) or polylactic acid (PLA) wound in a spool is continuously fed into an extruder that heats the material to its melting point and that moves on the horizontal plane across the printing tray to deposit the molten material in the spatial locations occupied by the printed object in each cross-section. Once the lowest cross-section of the object has been laid, the tray recedes or the extruder rises by one layer thickness (typically 0.1–0.4 mm) and the next layer is deposited. Printers can have a small number of extruders (typically 2–3), each printing with a different material (e.g., different colors or flexible and rigid). Surface finish is typically rough, commensurate with the lower resolution of this printing technology (0.2–0.4 mm).

Any one of the above technologies suffices to begin 3D printing anatomic models for surgical planning. In our lab we primarily use a consumer SLA printer with a 12.5×12.5×16.5 cm build tray and a layer resolution of up to 50μm (Form 1+, Formlabs, Somerville, MA). We prefer this technology due to the better surface finish and because complex geometries can be more easily printed compared to FDM. We construct multi-color models by printing each tissue separately with appropriate connectors introduced by CAD tools described above so as to snap-fit assemble the individual tissues into a single model. For larger and/or multi-material models we use outside services.

Implants and Prostheses

Powder bed fusion materials include synthetic polymers such as nylon, and metals and metal alloys such as titanium and cobalt-chrome all of which can be implanted. Recent research is developing bioresorbable polymers that can be used to 3D-print temporary implants using SLS [21]. As the name implies, the object is printed by selectively sintering or melting the surface of a powder bed of the material. SLS for example uses a high-power laser to selectively fuse particles in successive layers on the surface of the powder bed. A new thin layer of powder is laid after each cross-section of the model has been sintered. Finally, it is important to note that patient-specific implants can also be produced by molding using one of the anatomic model printing technologies described above to 3D-print the desired mold. While this is a multi-step process that requires specialized skills, it affords the opportunity to use other materials commonly used for implants such as polymethylmethacrylate (PMMA).

Printing & Post-Processing

It is important to note that all currently available 3D printing technologies require hours to produce a print. An aortic valve requires approximately 1.5 hours, a whole heart or the aortic wall from the aortic root to the level of the mid-descending aorta requires 6–8 hours, and an entire spine 16–24 hours. Time-to-print is dependent on the printing technology, model size and often material choice. A 3D-printed model also requires postprocessing. Post-processing involves both technology-specific steps such as final UV curing (e.g., SLA) or machining to polish (e.g., SLS), as well as the removal of support materials. For material jetting, SLA, and FDM supports are printed along with the desired model in order to support any overhangs in it. For binder jetting and powder bed fusion they are the excess powder underneath the overhangs that needs to be cleaned. Printed supports are most easily explained as follows. Printing a cube requires no supports as the material for the second print layer will find the material of the prior layer to rest upon. However, if the cube is partly hollow, printing the first layer of the top side of the cube is not possible as that layer would only be supported at the cube edges, where the side walls of the cube have been printed underneath. One cannot jet or deposit material elsewhere, as there is only empty space underneath. Support material is thus printed along with the model, in this case filling the cavity at all layers underneath the top side of the cube, thereby allowing print material to be deposited on it. Support removal is at least partly manual, often in conjunction with a water or other chemical bath.

At present, 3D printing of models strictly for surgical planning (as opposed to surgical guides and implants) is probably best achieved using any one of a number of commercial services such as Shapeways [22]. Although this avoids the manual labor involved in 3D printing, cost can be a limiting factor. 3D-printing two-three vertebral bodies can cost anywhere from $100-$700, while the entire ribcage and thoracic spine will cost roughly $2,000.

Imaging Considerations

High resolution, high-quality volumetric imaging is a prerequisite for 3D printing. CT and MRI are the most commonly used modalities as they are widely available and capable of providing isotropic 3D datasets with sufficient contrast to differentiate tissues of interest. Data acquired from additional imaging modalities can also be used for 3D printing in more limited scenarios. For example, 3D rotational angiography can be used when only intracardiac structures or the lumen of a vessel are required in a model [23, 24]. Alternatively, 3D ultrasound [25] including echocardiography [26] has been recently used to 3D-print models of cardiac structures.

Choosing the appropriate imaging modality and acquisition protocol to maximize tissue contrast, signal to noise ratio, and spatial resolution of a given anatomic area of interest increases the accuracy of the printed model and reduces the burden of the time-intensive segmentation and post-processing steps. This in turn facilitates integration of 3D printing into busy clinical workday schedules. For example, while CT allows for superior visualization of extracardiac and bony structures of the thorax, MRI offers better soft tissue delineation and is therefore superior for visualizing tumoral involvement of nerves or myocardial architecture. Similarly, echocardiography is superior for the visualization of

valvular structural and functional relationships [27]. Some of the imaging techniques reported for 3D printing of various tissues to date are summarized in Table 1. Even with an appropriately selected imaging modality, protocol details can simplify or complicate the 3D printing process. For example, in complex arteriovenous malformations, identification of abnormal vessels and early venous opacification on a single phase may indicate the clinical diagnosis. However, thin slices in multiple phases of contrast may be crucial in clearly identifying the feeding vessels for creating an accurate 3D-printed model. A common example we encounter is that while contrast injection in the upper extremity on the same side as that of an apical lung cancer does not limit diagnostic evaluation of the tumor itself, the resultant streak artifact from the dense contrast in the subclavian vein may limit spatial evaluation and accurate segmentation of the tumor relative to the adjacent relevant adjacent structures such as the subclavian artery, clavicle, and the first rib. In this case, addition of an unenhanced acquisition to the imaging protocol alleviates this issue.

Beyond innate tissue contrast, artifacts and signal-to-noise ratio are important factors to optimize. While thinner slices offer more accurate delineation of anatomy, the lower signal-to-noise ratio may limit or even prohibit segmentation of the tissues, particularly in the presence of streak or susceptibility artifact from metal when using CT or MRI data, respectively. For CT isotropic volumetric data should be reconstructed using slice thicknesses of 1–3 mm for thoracic 3D printing [28] and 0.5–1.25 mm for cardiac 3D printing [19, 29]. For CT, the selection of appropriate image reconstruction technique including reconstruction kernel and adaptive image reconstruction technologies can be used advantageously. Smooth kernels are preferred as they reduce noise, often simplifying segmentation. For example, 3D-printing of the costo-vertebral junction is simplified with slightly thicker slices (1.5 mm) and smooth kernel reconstruction, as partial voluming of the bone on both sides of the joint space enables segmentation to connect the vertebral body and head of the ribs, producing a single, connected 3D-printed model. Alternatively, as discussed earlier, this would necessitate additional CAD steps described, such as wrapping. Sharp kernels for CT reconstruction are preferred only when small structures are relevant for the model, such as small vessels [28, 30]. Often, reconstruction of CT images with both soft and sharp kernels and multiple slice thicknesses can be leveraged to adjust the segmentation and STL CAD manipulations while viewing all reconstructed images. In every case, the final STL models generated should be overlaid for verification onto each image set (Figure 3).

Future Directions

The accuracy of the 3D printed models used for patient care is a major concern. At present, 3D printers are sufficiently accurate with respect to clinically-relevant features, typically to <1 mm, and often less than the size of an imaging pixel [31–34]. However, a 3D printer is like any other instrument and must be maintained and calibrated at regular intervals to minimize anatomic discrepancies. Regular printing of "resolution phantoms" containing features of known dimensions can be used for preventive maintenance [28]. Such phantoms can also be printed along with each patient model to increase confidence of the individual model's accuracy.

The most important step for accuracy is likely segmentation, as maximal dimensional change for many STL manipulations can be manually controlled. We tend to enforce 1 imaging pixel size change for most STL manipulations such as wrapping. Tissue delineation on the other hand is subject to operator interpretation, and thus inter- and intra-observer variability will become a very important factor to assess in the future. This is further complicated by the lack of standardization of imaging protocols and segmentation approaches. For example, it is likely that a more reproducible segmentation of e.g., a chest wall sarcoma can be obtained from MR, with better differentiation from surrounding soft tissue compared to CT. Automated techniques to assess the effect of operator and choice of techniques for each of the four steps involved in 3D printing on model accuracy will be required before the technology is adopted into routine clinical practice.

Work is underway to develop these techniques and hence guide improvements in 3D-printing methodology. For example, we recently described an automated technique to quantify model variability by comparing the morphology of the difference between two STLs of a single tissue segmented from different image datasets (such as CT at different radiation doses) or by different operators [35]. Establishing accuracy will be more difficult than establishing reproducibility however, as there is limited opportunity to compare a printed model with the true patient anatomy. Cadaveric studies have been described [36–38] wherein printed models were compared to autopsy findings. Another opportunity is to compare the dimensions of tissue excised or visualized at surgery with those of the model [13], but the former depends on the completeness of excision and the latter is limited to areas/surfaces of tissues exposed in the surgical field as well as accurate measurement calibration that is often limited by the degree of access. While cumbersome and difficult to perform, such comparisons will nonetheless be necessary in the early stages of establishing the methods for 3D printing of clinical models.

Cardiovascular Applications

Many cardiovascular applications of 3D-printing are evident. The most widely reported application has been in congenital heart diseases (CHD). Applications for aortic and great vessel pathologies as well as cardiac valve disorders are also emerging. Simulation of both open heart surgery and catheter-based interventions is possible with current 3D printing technologies. The educational opportunities in this field are also quite promising. First-year medical students performed better in identifying cardiac anatomy when using models versus cadaveric materials for learning [18].

Higher spatial resolution (0.5–0.75 mm) is typically required. Additional challenges for 3D printing cardiovascular models include cardiac and breathing motion. Thus, classic techniques must be employed to ensure motion free images. This includes ECG-gating, breath-holding, and potentially respiratory gating for MR angiography (MRA). Presence of arrhythmias inevitably limits the feasibility of printing an exam just as it limits its diagnostic capacity [39]. Whenever tissue architecture is not required, such as for endovascular procedure planning, any 3D angiographic modality can be used, including CT angiography (CTA), MRA, and 3D rotational angiography. Models of the intracardiac structure and vessel lumen can be printed by creating a fictitious wall around the contrast enhanced blood pool

that is segmented from the angiogram (Figure 3). 3D echocardiography, CT, and MR have been used for models of tissue architecture [40–42]. Both hard and flexible models or models combining both types of materials can be printed with sufficiently realistic properties compared to tissue to enable physicians to perform mock surgeries and percutaneous interventions toward better-appreciating potential procedural difficulties, assessing the likelihood of success or failure, and selecting appropriate instrumentation (Figure 4).

Congenital heart diseases

Although anatomical features enable classification of CHD into broad categories, treatment strategies and prognoses are heavily dependent on patient-specific anatomical variations. This has led to 3D printing quickly becoming indispensable in CHD for both surgical planning and training. Medical students exhibited significant improvement in knowledge acquisition, knowledge reporting and structural conceptualization when using 3D-printed models as learning aids for CHD anatomy [43], and at least one effort is underway to create a library of 3D-printed CHD models (http://imib-chd.com) [44] to facilitate increased proficiency in the full spectrum of CHDs.

Septal defects, both atrial (ASD) and ventricular (VSD), are amongst the most frequently printed pathologies to assist with intra-operative spatial navigation and patch sizing. They are relatively simple to print from contrast-enhanced CT, MRI and more recently, echocardiography [3, 17, 40, 41, 45–47]. Kim *et al.* reported the utility of 3D printed models for occluder device sizing and selection of the approach to cross the defect in cases of a muscular VSD and a fenestrated ASD with a large atrial septal aneurysm [48]. Separate models of the intracardiac volumes (blood pool) and the myocardium plus vessel walls were reported for a complicated case of a patient with transposition of great vessels, large VSD, ASD and dextrocardia that had undergone a number of prior surgical interventions [5]. Using the physical models in the operating room, surgeons could readily identify the location of the coronaries from the blood pool model while the muscle model enabled clear delineation of the VSD in physiologic conditions (Figure 5). The complementary nature of blood pool and organ tissue models applies to most vascular pathologies (Figure 6), as the former enables quick appreciation of the shape and size of the pathology, while the latter can either be cut open to aid in visualizing the planned surgical approach or used to simulate a catheter-based procedure. To this end, the ability to print models in transparent, flexible material that can be cut and bent allowing for inspection and assessment of pathology, and selection of optimal viewing planes for complicated cases has been a significant advance in cardiovascular 3D printing [49].

Echocardiography is used for routine imaging of CHD. Recent research efforts have enabled it to be used to reliably 3D-print anatomic models. Olivieri *et al.* generated 3D printed models of 8 patients with VSDs from subcostal view transthoracic echocardiography (TTE) images with high correlation and accuracy of long and short-axis measurements between the printed models and conventional 2D echocardiographic measurements [40]. Another group 3D-printed an ostium secundum ASD using images from transesophageal echocardiography (TEE) which improved visualization of the defect viewed from the left atrium [50]. 3D printing from echocardiographic images involves segmenting the myocardium directly as

opposed to e.g., CTA and MRA where the contrast enhanced blood pool is more readily segmented and a fictitious myocardial wall is typically created around it to visualize intracardiac structures. For echocardiography, low noise in the dark blood pool is key, and both we and others have employed noise reduction and smoothing filters to de-speckle the images to simplify segmentation. Finally, the typical tradeoff between optimizing field-of-view and temporal resolution to mitigate cardiac motion applies in 3D printing as for diagnosis.

Specifically for patients scheduled to undergo catheter-based procedures, 3D printed models are likely to help reduce fluoroscopy time and thus radiation and contrast exposure. Ryan *et al.* [51] opted for a minimal-radiation cardiac CT at the first day of life of a patient with Tetralogy of Fallot with pulmonary atresia and multiple aortopulmonary collaterals. The 3D-printed model improved planning of placement of a central aortopulmonary shunt and subsequent coiling of redundant collateral vessels. The entirety of a stent deployment can be simulated in printed models, which are typically radiopaque and visible under fluoroscopy. Pathologies for which this has been utilized include a case of hypoplastic transverse aortic arch [52], and a case of pulmonary venous baffle obstruction of a patient post Mustard operation for D-Transposition of Great Vessels [53]. Figure 7 shows a model derived from a delayed phase CTA created to determine feasibility of revising the Mustard baffles in a high surgical risk patient with leaks not amenable to transcatheter device closure. The 3D printed model clearly depicted two large and one smaller leak in the inferior and superior aspect of the baffle. Procedure simulation revealed that telescoping thoracic grafts and abdominal grafts were most appropriate for the inferior and superior baffles, respectively.

Pre-operative simulation and intraoperative navigation applications described above are uniquely enabled by 3D printing. It is also more effective than review of imaging findings in efficiently conveying information. In a study of 12 patients with pulmonary valve abnormalities evaluated for percutaneous pulmonary valve implantation versus surgical correction, printed models of the right ventricle outflow tract (RVOT) and pulmonary bifurcation were retrospectively assessed by cardiologists blinded to the treatment approach. Patient selection for the percutaneous approach was more accurate when physicians evaluated the physical models compared to the MRI images alone [54].

Cardiac Valves and other Structural Diseases

3D printing of the aortic valve remains an actively-researched field, aimed at developing functionally accurate models. Current results suggest that 3D-printed models may offer an incremental benefit for transcatheter aortic valve replacement (TAVR) planning. A retrospective study simulated TAVR in 3D printed models containing both flexible material for the vessel wall and rigid material for calcifications. Deployment of the same device into the 3D model as implanted in the patient was reported to improve anticipation of potential difficulties and to have the potential to help minimize peri- and post-operative complications [7]. More recently, we reported the use of flexible 3D printed models of the aortic root complex derived from routine TAVR planning CT angiography to predict perivalvular leak in a small series of patients [11]. 3D printed models of the implanted valves (26 or 29 mm Edwards SAPIEN XT in this patient series) with a closed configuration and corresponding

to the valve implanted in each patient were carefully positioned in the patient's printed aortic root model. A focused light was then projected through the LVOT to assess any leakage through the closed valve model, which if present was considered predictive of a perivalvular leak. Leaks were correctly identified in 6 of 9 patients and correctly ruled out in 5 of 7 patients compared to the patient's post-procedural TTE. The shape and location of light passing through the model with the implanted valve accurately matched the leak location identified in the TTE. The aortic models in this study excluded valve leaflets, as they are difficult to segment from CTA. However, these will be essential in printing functionally realistic cardiac valve models.

Work in this area has recently yielded 3D-printed models of aortic valves with severe aortic stenosis from CTA that are functionally similar with respect to spectral Doppler measurements [55]. In vitro flow experiments on the models replicated hemodynamic values (aortic valve area and mean and peak transvalvular pressure gradient) with good correlation (Pearson r>0.97) compared to *in vivo* Doppler measurements (Figure 8). In other cases, where the cusps are more mobile, existing 3D printing processes are suboptimal for modeling pathologies such as valve regurgitation, as most 3D printing material have different stress-strain relationships than human tissue. Encouraging results from multi-material 3D printing [56, 57] may nonetheless soon alleviate this issue.

3D printing is expected to be instrumental in the development of minimally invasive mitral valve replacement procedures, the next major frontier in interventional structural heart procedures following the now well-established TAVR procedure [58, 59]. Early 3D printing efforts of the mitral valve apparatus have primarily used TEE [26, 60, 61]. The mitral valve apparatus is exquisitely complex including the left atrial and ventricular wall, the annulus, the leaflets, the chordae tendineae and the papillary muscles. The lack of appropriate materials to mimic their mechanical complexity at present limits application of the technology to education and visualization of pathology. Accurate models of the mitral valve printed at multiple time points throughout the cardiac cycle may help to better appreciate the valve geometry and function, and to perform more accurate measurements than possible intra-operatively on a non-beating heart (Figure 9). Mahmood *et al.* reported specialized commercial TEE software to segment the mitral annulus [26] and subsequently the leaflets [62]. Witschey *et al.* [61], similarly printed models of mitral valves of normal and ischemic mitral regurgitation and myxomatous degeneration from 3D TEE images using a semi-automated segmentation method (Figure 10). The mitral annulus could be printed in 30 min and the entire valve within 90 min, with the bulk likely expended on the printing time. Specialized automated software in this and many other applications in the future will be key in reducing the segmentation burden for 3D printing that currently limits clinical application.

Other than the aortic and mitral valves, 3D printing of the right atrium-IVC junction has also been reported to assist with sizing a caval valve implantation in a patient with secondary tricuspid regurgitation [63]. As more functionally accurate 3D printing becomes a reality, device testing and minimally invasive procedure simulations will follow. At present we are considering the use of experiments with flow in the printed models under fluoroscopy to help prepare for transcatheter mitral valve replacement [64]. In the future, patient-specific annuloplasty devices and prosthetic heart valves could become a possibility [65].

The use of 3D-printed models of the blood pool and myocardium extends beyond the valves. A model of the right ventricular outflow tract assisted pulmonary valve implantation [24]. Intracardiac structure models were used in a case of severe prosthetic mitral valve leak to assist percutaneous implantation of an occluder device to cover the valve defect [48]. The latter model assisted in selecting the appropriate delivery approach and device size that would not interfere with the adjacent prosthetic valve struts. Myocardial tissue models have been used for planning resections in two cases of left ventricular aneurysms and a case of right ventricular tumor [29]. The models aided in identifying structures at risk, assessment of ideal resection lines, and planning the ideal residual shape after reconstruction. A recent application of multi-color 3D-printed models of cardiac tissue is guidance of septal myectomy for hypertrophic cardiomyopathy [42]. Printed models can offer unparalleled visualization of the myocardium, intraventricular muscle band, accessory papillary muscle and mitral annulus in different colors and in flexible materials that offer haptic feedback which resembles the intraoperative approach. Models including both the heart and adjacent thoracic structures can be useful for planning surgery in patients with prior interventions, where anatomy may deviate from that expected. Such a 3D-printed model has been reported to assist in protecting a patent coronary bypass graft and other cardiac structures in a patient with previous CABG that required resternotomy for open aortic valve repair [6].

Great vessels

3D printing of hollow models of the vascular lumen can aid in procedure selection, diagnosis, and device testing. The ascending aorta and aortic arch are of particular interest here. A model was reported for planning and simulating transcatheter delivery of an occluder device to an aortic arch pseudoaneurysm [66]. We have found 3D-printed models to be useful in cases of mobile atheromas identified with TEE in the aortic arch and proximal descending aorta, assisting comprehension of the location of the lesions, their proximity to the aortic arch vessels and assessing the feasibility of endovascular repair (Figure 11). 3D-printing of the abdominal aorta can be useful in complex cases such as an abdominal aortic aneurysm with complex neck anatomy where a printed model facilitated endovascular repair with regards to device selection and stent-graft delivery [67]. A model of a descending aorta with a pseudoaneurysm and multifocal ulcerations enabled endoprothesis size selection and accurate delivery covering both the rupture location and ulcerations [48]. An example of the added value of 3D printing toward optimizing operating room time was illustrated by the development of personalized external aortic root support for Marfan syndrome patients. Printed models of a patient's aorta from the annulus to the proximal aortic arch were used to knit a bespoke sleeve support [68] which can then be surgically implanted [12].

Thoracic applications

Although most thoracic applications of 3D printing are demanding in terms of both image segmentation and printing time, they are rapidly gaining traction. More expensive 3D printers with larger build trays are necessary for most applications. Models have been reported to assist in diagnosis and treatment of complex airway diseases, and neurosurgical and orthopedic surgical planning. CT and MRI are most commonly used, as a large field-of-view and good tissue contrast are necessary. Resolution can be sacrificed given the larger

organs and pathologies involved. Multiple contrast weightings in MR and both contrast enhanced and unenhanced CT acquisitions (and potentially in the future dual-energy CT [69]) are useful to differentiate all the involved tissues. Finally, a recent exciting application of 3D printing in the thoracic arena is the direct printing of both permanent and bioresorbable implants.

Tracheobronchial tree

3D printed models of the airways are likely useful only for complex cases and as training models. Tam *et al.*, printed the tracheobronchial tree of a patient with advanced relapsing polychondritis complicated by tracheobronchial chondromalacia [8] (Figure 12). Similar to static models of the cardiac valves printed at multiple points in the cardiac cycle to aid planning, 3D printing of the diseased airways in both expiration and inspiration from appropriately timed image acquisitions can enhance comprehension of the extent and location of disease to aid stenting procedures. A model of the bronchial tree in a post-lung transplantation patient with stenosis of the proximal portion of the bronchus intermedius enabled planning a modified silicone stent insertion with appropriate sizing of the orifice for the upper lobe airway [70]. A 3D printed model enabled experimentation with different-sized tracheal tubes in preparation for a challenging intubation of a 6yo child that required sequential single-lung ventilation for whole-lung lavage [71] (Figure 13). 3D-printed models of anatomical variants of the tracheobronchial tree have also been reported toward enhancing flexible bronchoscopy proficiency [72].

A recent ground-breaking application was described wherein 3D-printed bioresorbable tracheal splints were implanted in infants with life-threatening tracheomalacia [21]. The splints were precisely printed to fit the individual patient's anatomy so as to prevent airway collapse during expiration, and, in one case, to accommodate concurrent use of both left and right bronchial splints. The splints were designed with a 90-degree circumferential gap to both allow insertion over the airway and to accommodate distention in tandem with physiologic growth with age. The splints were printed with a commercial SLS printer using polycaprolactone, a biocompatible, bioresorbable material with resorption time close to 3 years.

Spine & Chest Wall

Vertebral bodies can be printed accurately and reproducibly from non-contrast CT with minimal segmentation effort [38, 73] given the high tissue-bone contrast, and their utility in corrective surgery is rapidly being assessed. A large-scale study in 126 adolescent idiopathic scoliosis patients used 3D printed models of the entire spine to plan the corrective procedure, identifying complex or abnormal structures and simulating screw implantation. The models had no effect on complication rates, postoperative radiological outcomes or length of hospital stay, and resulted in a 3% overall increase in cost per patient. However, operating room (OR) time was reduced by 13% (184 versus 212 min with versus without models) and blood loss was reduced by 18% [14]. This perhaps highlights an administrative incentive for introducing a clinical 3D printing service in an academic hospital at present, namely performing more operations in a day without reducing the quality of care.

In the future, modeling soft tissues surrounding the vertebrae may confer further benefits by enabling better evaluation of the relationship between planned screw fixation and soft tissues. In our institution we are developing material jetting 3D-printed models that can generate an MRI signal toward simulating MRI-guided procedures such as cryosurgeries [74]. Simulating the procedure using these models under MRI surveillance can help determine the optimal drill trajectory to ablate the tumor while avoiding adjacent tissues, such as the spinal nerves in a case of a spinal osteoid osteoma. We anticipate that in the near future we will be able to print models that when imaged with MRI will depict the patient's nerves, bone, tumor, fat and cerebrospinal fluid in different signal intensities, resulting in printed phantoms with accurate reproduction of human MRI anatomy.

Beyond anatomic models for procedure planning, 3D printing using biocompatible materials offers a unique opportunity to *a priori* create bone drilling guides. This can potentially further reduce OR time by shifting procedure burden to pre-operative modeling. Sugawara *et al.* reported the creation of posterior thoracic pedicle fixation screw guiding structures to fit each lamina for a set of ten patients with thoracic or cervicothoracic pathological entities [75]. The patient-specific guides were sterilized with a plasma sterilizer for intraoperative use. Postoperative evaluation using CT showed a mean deviation of the screws from their planned trajectories of 0.87 ± 0.34 mm at the coronal midpoint section of the pedicles.

An important application of 3D-printed implants that is actively sought is chest wall reconstruction. Titanium plates and bars are commonly utilized and thus regulatory burdens toward moving to patient-specific titanium implants that are 3D-printed are reduced, particularly when using 510(k)-cleared 3D-printing software such as the Mimics suite (Materialise, Leuven, Belgium). Early reports are already appearing toward improving cosmetic results without compromising protection or respiratory mechanics. Aranda *et al.* reported the implantation of a 3D-printed titanium rigid sternal core with rods as neo-ribs ending in clamps to attach to the costal stumps for a patient with an 8×8 cm parasternal mass with involvement of both pectoral muscles, sternal body and third and fourth bilateral ribs [16] (Figure 14).

Lung and Mediastinum

3D printing is invaluable for the patient with complex or anomalous anatomy undergoing thoracic surgery. Akiba *et al.* 3D-printed the bronchi and pulmonary artery and veins of a patient with variant anatomy of the right upper lobe bronchus who underwent a thoracoscopic anterior segmentectomy and middle lobectomy for lung cancer [9]. Dickinson *et al.* reported 2 cases of complex esophageal pathology where extensive 3D-printed models (in one case including esophagus and fistulous tract, spit fistula, stomach, aorta and aortic graft, trachea, veins, diaphragmatic crus, spine and ribs) helped define the surgical approach [76]. In the first patient with left pneumonectomy, aortic bypass and esophageal diversion that required esophageal endomucosal resection and gastroesophageal junction stapling, the model enabled assessment of the proximity of the esophagus to the aortic graft and pre-operative simulation and intraoperative guidance for a hybrid endoscopic-surgical approach that would otherwise not have been attempted. In the second patient with multiple esophageal diverticula (Figure 15), the model led to the selection of a laparoscopic approach

rather than a thoracoscopic approach for an esophageal myotomy and diverticulectomy. Both cases additionally highlight the importance of carefully optimizing the imaging protocol to separate the structures of interest. In this work, the authors used a positive enteric contrast agent (iodinated contrast or barium) in combination with effervescent granules to distend and visualize the otherwise collapsed esophageal lumen.

We have found 3D-printed models extremely useful for certain thoracic tumors that present surgical challenges due to their intrinsic location and proximity to vascular structures, even in the absence of individual patient anatomical variations. In our experience, 3D-printed models including the tumor, adjacent bones, and nearby systemic and pulmonary vasculature created from CT and MRI contribute to at least similar if not improved comprehension of anatomic relationships by surgeons. We also extensively use models for communicating the surgical plan amongst multispecialty surgical teams. Two examples, a superior sulcus (Pancoast) and a mediastinal tumor are shown in Figures 16 and 17. In a series of two Pancoast tumor patients, our surgeons felt that the models were superior (defined as similar information assimilated more rapidly, or providing additional conceptual information) to 2D images and 3D reconstructions for assessing resectability, selecting the surgical approach and understanding tumor relationship to vessels. Although there was minimal or moderate self-reported perceived decrease in OR time, a cost benefit may still be incurred since surgical planning, for which there was a significant benefit using the models, is a considerable component of overall resource utilization in these cases. Larger studies will be needed to establish whether there are additional patient benefits in terms of peri- and post-operative complications as well as the utility of the models in enhancing patient understanding of the procedure and aiding the informed consent process.

Conclusion

Medical 3D printing holds great promise towards improving medical care. The application of this technology in medical practice is still in its infancy. Thus, although there are inflated expectations by some, and skepticism by others, the current stage is best described as that of the "innovation trigger". In this phase, new, useful applications are being quickly developed that may enhance or completely shift the paradigm for cardiothoracic interventions. Reports of applications in research, education, and surgical and interventional planning and simulation are quickly increasing. For the near term, application of 3D-printing in clinical practice will hinge on identification of proper indications with regards to cost-benefit ratios, standardization of the workflow for the steps involved in 3D-printing DICOM images, and governmental approvals to facilitate the use of 3D-printed patient-specific implants.

Acknowledgments

References

1. Markl M, Schumacher R, Kuffer J, et al. Rapid vessel prototyping: vascular modeling using 3t magnetic resonance angiography and rapid prototyping technology. MAGMA. 2005; 18(6):288–92. [PubMed: 16369802]

2. McGurk M, Amis AA, Potamianos P, et al. Rapid prototyping techniques for anatomical modelling in medicine. Annals of The Royal College of Surgeons of England. 1997; 79(3):169–174. [PubMed: 9196336]

3. Noecker AM, Chen JF, Zhou Q, et al. Development of patient-specific three-dimensional pediatric cardiac models. ASAIO J. 2006; 52(3):349–53. [PubMed: 16760727]

4. Schievano S, Sala G, Migliavacca F, et al. Use of rapid prototyping models in the planning of percutaneous pulmonary valved stent implantation. Proceedings of the Institution of Mechanical Engineers, Part H: Journal of Engineering in Medicine. 2007; 221(4):407–416.

5. Mottl-Link S, Hubler M, Kuhne T, et al. Physical models aiding in complex congenital heart surgery. Ann Thorac Surg. 2008; 86(1):273–7. [PubMed: 18573436]

6. Sodian R, Schmauss D, Markert M, et al. Three-dimensional printing creates models for surgical planning of aortic valve replacement after previous coronary bypass grafting. Ann Thorac Surg. 2008; 85(6):2105–8. [PubMed: 18498831]

7. Schmauss D, Schmitz C, Bigdeli AK, et al. Three-dimensional printing of models for preoperative planning and simulation of transcatheter valve replacement. Ann Thorac Surg. 2012; 93(2):e31–3. [PubMed: 22269765]

8. Tam MD, Laycock SD, Jayne D, et al. 3-D printouts of the tracheobronchial tree generated from CT images as an aid to management in a case of tracheobronchial chondromalacia caused by relapsing polychondritis. J Radiol Case Rep. 2013; 7(8):34–43. [PubMed: 24421951]

9. Akiba T, Inagaki T, Nakada T. Three-dimensional printing model of anomalous bronchi before surgery. Ann Thorac Cardiovasc Surg. 2014; 20(Suppl):659–62. [PubMed: 24088921]

10. Maragiannis D, Jackson MS, Igo SR, et al. Functional 3D printed patient-specific modeling of severe aortic stenosis. J Am Coll Cardiol. 2014; 64(10):1066–8. [PubMed: 25190245]

11. Ripley B, Kelil T, Cheezum MK, et al. 3D printing based on cardiac CT assists anatomic visualization prior to transcatheter aortic valve replacement. J Cardiovasc Comput Tomogr. 2015

12. Treasure T, Takkenberg JJ, Golesworthy T, et al. Personalised external aortic root support (PEARS) in Marfan syndrome: analysis of 1–9 year outcomes by intention-to-treat in a cohort of the first 30 consecutive patients to receive a novel tissue and valve-conserving procedure, compared with the published results of aortic root replacement. Heart. 2014; 100(12):969–75. [PubMed: 24395977]

13. Weinstock P, Prabhu SP, Flynn K, et al. Optimizing cerebrovascular surgical and endovascular procedures in children via personalized 3D printing. Journal of Neurosurgery: Pediatrics. 2015; 16(5):584–589.

14. Yang M, Li C, Li Y, et al. Application of 3D rapid prototyping technology in posterior corrective surgery for Lenke 1 adolescent idiopathic scoliosis patients. Medicine (Baltimore). 2015; 94(8):e582. [PubMed: 25715261]

15. Zopf DA, Flanagan CL, Wheeler M, et al. Treatment of severe porcine tracheomalacia with a 3-dimensionally printed, bioresorbable, external airway splint. JAMA Otolaryngol Head Neck Surg. 2014; 140(1):66–71. [PubMed: 24232078]

16. Aranda JL, Jimenez MF, Rodriguez M, et al. Tridimensional titanium-printed custom-made prosthesis for sternocostal reconstruction. Eur J Cardiothorac Surg. 2015; 48(4):e92–4. [PubMed: 26242897]

17. Giannopoulos AA, Chepelev L, Sheikh A, et al. 3D printed ventricular septal defect patch: a primer for the 2015 Radiological Society of North America (RSNA) hands-on course in 3D printing. 3D Printing in Medicine. 2015; 1(1)

18. Lim KH, Loo ZY, Goldie SJ, et al. Use of 3D printed models in medical education: A randomized control trial comparing 3D prints versus cadaveric materials for learning external cardiac anatomy. Anat Sci Educ. 2015

19. Mitsouras D, Liacouras P, Imanzadeh A, et al. Medical 3D Printing for the Radiologist. Radiographics. 2015; 35(7):1965–88. [PubMed: 26562233]

20. Russ, M.; O'Hara, R.; Setlur Nagesh, SV., et al. Treatment planning for image-guided neuro-vascular interventions using patient-specific 3D printed phantoms. Proc SPIE Int Soc Opt Eng; 2015; Orlando, FL.

21. Morrison RJ, Hollister SJ, Niedner MF, et al. Mitigation of tracheobronchomalacia with 3D-printed personalized medical devices in pediatric patients. Sci Transl Med. 2015; 7(285):285ra64.

22. Shapeways. Shapeways. 2016. [cited 2016 1]; Available from: http://www.shapeways.com/

23. Ionita, CN.; Suri, H.; Nataranjian, S., et al. Angiographic imaging evaluation of patient-specific bifurcation-aneurysm phantom treatment with pre-shaped, self-expanding, flow-diverting stents: feasibility study. Proceedings of SPIE--the International Society for Optical Engineering; 2011; p. 79651H-1-79651H-9.

24. Poterucha JT, Foley TA, Taggart NW. Percutaneous pulmonary valve implantation in a native outflow tract: 3-dimensional DynaCT rotational angiographic reconstruction and 3-dimensional printed model. JACC Cardiovasc Interv. 2014; 7(10):e151–2. [PubMed: 25341717]

25. Gatto M, Memoli G, Shaw A, et al. Three-Dimensional Printing (3DP) of neonatal head phantom for ultrasound: Thermocouple embedding and simulation of bone. Medical Engineering & Physics. 2012; 34(7):929–937. [PubMed: 22105079]

26. Mahmood F, Owais K, Taylor C, et al. Three-dimensional printing of mitral valve using echocardiographic data. JACC Cardiovasc Imaging. 2015; 8(2):227–9. [PubMed: 25457770]

27. Kurup HK, Samuel BP, Vettukattil JJ. Hybrid 3D printing: a game-changer in personalized cardiac medicine? Expert Rev Cardiovasc Ther. 2015; 13(12):1281–4. [PubMed: 26465262]

28. Matsumoto JS, Morris JM, Foley TA, et al. Three-dimensional Physical Modeling: Applications and Experience at Mayo Clinic. Radiographics. 2015; 35(7):1989–2006. [PubMed: 26562234]

29. Jacobs S, Grunert R, Mohr FW, et al. 3D-Imaging of cardiac structures using 3D heart models for planning in heart surgery: a preliminary study. Interact Cardiovasc Thorac Surg. 2008; 7(1):6–9. [PubMed: 17925319]

30. Flohr TG, Schoepf UJ, Ohnesorge BM. Chasing the heart: new developments for cardiac CT. J Thorac Imaging. 2007; 22(1):4–16. [PubMed: 17325571]

31. Nizam A, Gopal RN, Naing L, et al. Dimensional accuracy of the skull models produced by rapid prototyping technology using stereolithography apparatus. Orofacial Sciences. 2006; 1:60–6.

32. Salmi M, Paloheimo KS, Tuomi J, et al. Accuracy of medical models made by additive manufacturing (rapid manufacturing). J Craniomaxillofac Surg. 2013; 41(7):603–9. [PubMed: 23333490]

33. Taft RM, Kondor S, Grant GT. Accuracy of rapid prototype models for head and neck reconstruction. J Prosthet Dent. 2011; 106(6):399–408. [PubMed: 22133397]

34. Waran V, Devaraj P, Hari Chandran T, et al. Three-dimensional anatomical accuracy of cranial models created by rapid prototyping techniques validated using a neuronavigation station. J Clin Neurosci. 2012; 19(4):574–7. [PubMed: 22305869]

35. Cai T, Rybicki F, Giannopoulos A, et al. The residual STL volume as a metric to evaluate accuracy and reproducibility of anatomic models for 3D printing: application in the validation of 3D-printable models of maxillofacial bone from reduced radiation dose CT images. 3D. Printing in Medicine. 2015; 1(1):2.

36. Ebert LC, Thali MJ, Ross S. Getting in touch--3D printing in forensic imaging. Forensic Sci Int. 2011; 211(1–3):e1–6. [PubMed: 21602004]

37. Schievano S, Sebire NJ, Robertson NJ, et al. Reconstruction of fetal and infant anatomy using rapid prototyping of post-mortem MR images. Insights Imaging. 2010; 1(4):281–286. [PubMed: 22347922]

38. Ogden KM, Aslan C, Ordway N, et al. Factors Affecting Dimensional Accuracy of 3-D Printed Anatomical Structures Derived from CT Data. J Digit Imaging. 2015; 28(6):654–63. [PubMed: 25982877]

39. Techasith T, Ghoshhajra BB, Truong QA, et al. The effect of heart rhythm on patient radiation dose with dual-source cardiac computed tomography. Journal of Cardiovascular Computed Tomography. 2011; 5(4):255–263. [PubMed: 21723517]

40. Olivieri LJ, Krieger A, Loke YH, et al. Three-dimensional printing of intracardiac defects from three-dimensional echocardiographic images: feasibility and relative accuracy. J Am Soc Echocardiogr. 2015; 28(4):392–7. [PubMed: 25660668]

41. Riesenkampff E, Rietdorf U, Wolf I, et al. The practical clinical value of three-dimensional models of complex congenitally malformed hearts. J Thorac Cardiovasc Surg. 2009; 138(3):571–80. [PubMed: 19698837]

42. Yang DH, Kang JW, Kim N, et al. Myocardial 3-Dimensional Printing for Septal Myectomy Guidance in a Patient With Obstructive Hypertrophic Cardiomyopathy. Circulation. 2015; 132(4): 300–1. [PubMed: 26216088]

43. Costello JP, Olivieri LJ, Krieger A, et al. Utilizing Three-Dimensional Printing Technology to Assess the Feasibility of High-Fidelity Synthetic Ventricular Septal Defect Models for Simulation in Medical Education. World J Pediatr Congenit Heart Surg. 2014; 5(3):421–426. [PubMed: 24958045]

44. 3DHopeMedical. 2016. http://imib-chd.com/cited 2016 1

45. Schmauss D, Haeberle S, Hagl C, et al. Three-dimensional printing in cardiac surgery and interventional cardiology: a single-centre experience. Eur J Cardiothorac Surg. 2015; 47(6):1044–52. [PubMed: 25161184]

46. Shiraishi I, Kurosaki K, Kanzaki S, et al. Development of Suepr Flexible Replica of Congenital Heart Disease with Stereolithography 3D Printing for Simulation Surgery and Medical Education. Journal of Cardiac Failure. 2014; 20(10):S180–S181.

47. Shiraishi I, Yamagishi M, Hamaoka K, et al. Simulative operation on congenital heart disease using rubber-like urethane stereolithographic biomodels based on 3D datasets of multislice computed tomography. Eur J Cardiothorac Surg. 2010; 37(2):302–6. [PubMed: 19758813]

48. Kim MS, Hansgen AR, Wink O, et al. Rapid prototyping: a new tool in understanding and treating structural heart disease. Circulation. 2008; 117(18):2388–94. [PubMed: 18458180]

49. Schrot J, Pietila T, Sahu A. State of the art: 3D printing for creating compliant patient-specific congenital heart defect models. Journal of Cardiovascular Magnetic Resonance. 2014; 16(Suppl 1):W19.

50. Faganello G, Campana C, Belgrano M, et al. Three dimensional printing of an atrial septal defect: Is it multimodality imaging? Int J Cardiovasc Imaging. 2015

51. Ryan JR, Moe TG, Richardson R, et al. A novel approach to neonatal management of tetralogy of Fallot, with pulmonary atresia, and multiple aortopulmonary collaterals. JACC Cardiovasc Imaging. 2015; 8(1):103–4. [PubMed: 25457761]

52. Valverde I, Gomez G, Coserria JF, et al. 3D printed models for planning endovascular stenting in transverse aortic arch hypoplasia. Catheter Cardiovasc Interv. 2015; 85(6):1006–12. [PubMed: 25557983]

53. Olivieri L, Krieger A, Chen MY, et al. 3D heart model guides complex stent angioplasty of pulmonary venous baffle obstruction in a Mustard repair of D-TGA. Int J Cardiol. 2014; 172(2):e297–8. [PubMed: 24447757]

54. Schievano S, Migliavacca F, Coats L, et al. Percutaneous pulmonary valve implantation based on rapid prototyping of right ventricular outflow tract and pulmonary trunk from MR data. Radiology. 2007; 242(2):490–7. [PubMed: 17255420]

55. Maragiannis D, Jackson MS, Igo SR, et al. Replicating Patient-Specific Severe Aortic Valve Stenosis With Functional 3D Modeling. Circ Cardiovasc Imaging. 2015; 8(10)

56. Wang K, Zhao Y, Chang Y-H, et al. Controlling the mechanical behavior of dual-material 3D printed meta-materials for patient-specific tissue-mimicking phantoms. Materials & Design. 2016; 90:704–712.

57. Biglino G, Verschueren P, Zegels R, et al. Rapid prototyping compliant arterial phantoms for in-vitro studies and device testing. J Cardiovasc Magn Reson. 2013; 15:2. [PubMed: 23324211]

58. Holmes DR Jr, Mack MJ, Kaul S, et al. 2012 ACCF/AATS/SCAI/STS Expert Consensus Document on Transcatheter Aortic Valve Replacement. Journal of the American College of Cardiology. 2012; 59(13):1200–1254. [PubMed: 22300974]

59. Achenbach S, Delgado V, Hausleiter J, et al. SCCT expert consensus document on computed tomography imaging before transcatheter aortic valve implantation (TAVI)/transcatheter aortic

valve replacement (TAVR). Journal of Cardiovascular Computed Tomography. 2012; 6(6):366–380. [PubMed: 23217460]

60. Kapur KK, Garg N. Echocardiography derived three- dimensional printing of normal and abnormal mitral annuli. Ann Card Anaesth. 2014; 17(4):283–4. [PubMed: 25281625]

61. Witschey WR, Pouch AM, McGarvey JR, et al. Three-dimensional ultrasound-derived physical mitral valve modeling. Ann Thorac Surg. 2014; 98(2):691–4. [PubMed: 25087790]

62. Mahmood F, Owais K, Montealegre-Gallegos M, et al. Echocardiography derived three-dimensional printing of normal and abnormal mitral annuli. Ann Card Anaesth. 2014; 17(4):279–83. [PubMed: 25281624]

63. O'Neill B, Wang DD, Pantelic M, et al. Transcatheter caval valve implantation using multimodality imaging: roles of TEE, CT, and 3D printing. JACC Cardiovasc Imaging. 2015; 8(2):221–5. [PubMed: 25677894]

64. Izzo, RL.; O'Hara, RP.; Iyer, V., et al. SPIE Medical Imaging. San Diego, California, United States: 2016. 3D printed cardiac phantom for procedural planning of a transcatheter native mitral valve replacement.

65. Cheung DY, Duan B, Butcher JT. Current progress in tissue engineering of heart valves: multiscale problems, multiscale solutions. Expert Opin Biol Ther. 2015; 15(8):1155–72. [PubMed: 26027436]

66. Sodian R, Schmauss D, Schmitz C, et al. 3-dimensional printing of models to create custom-made devices for coil embolization of an anastomotic leak after aortic arch replacement. Ann Thorac Surg. 2009; 88(3):974–8. [PubMed: 19699931]

67. Tam MDBS, Laycock SD, Brown JRI, et al. 3D Printing of an Aortic Aneurysm to Facilitate Decision Making and Device Selection for Endovascular Aneurysm Repair in Complex Neck Anatomy. Journal of Endovascular Therapy. 2013; 20(6):863–867. [PubMed: 24325705]

68. Izgi C, Nyktari E, Alpendurada F, et al. Effect of personalized external aortic root support on aortic root motion and distension in Marfan syndrome patients. Int J Cardiol. 2015; 197:154–60. [PubMed: 26134372]

69. Machida H, Tanaka I, Fukui R, et al. Current and Novel Imaging Techniques in Coronary CT. RadioGraphics. 2015; 35(4):991–1010. [PubMed: 26046942]

70. Miyazaki T, Yamasaki N, Tsuchiya T, et al. Airway stent insertion simulated with a three-dimensional printed airway model. Ann Thorac Surg. 2015; 99(1):e21–3. [PubMed: 25555984]

71. Wilson CA, Arthurs OJ, Black AE, et al. Printed three-dimensional airway model assists planning of single-lung ventilation in a small child. Br J Anaesth. 2015; 115(4):616–20. [PubMed: 26385670]

72. Bustamante S, Bose S, Bishop P, et al. Novel application of rapid prototyping for simulation of bronchoscopic anatomy. J Cardiothorac Vasc Anesth. 2014; 28(4):1122–5. [PubMed: 24332921]

73. Wu AM, Shao ZX, Wang JS, et al. The accuracy of a method for printing three-dimensional spinal models. PLoS One. 2015; 10(4):e0124291. [PubMed: 25915641]

74. Mitsouras D, Lee TC, Liacouras P, et al. Three-dimensional printing of MRI-visible phantoms and MR image-guided therapy simulation. Magnetic Resonance in Medicine. 2016 n/a-n/a.

75. Sugawara T, Higashiyama N, Kaneyama S, et al. Multistep pedicle screw insertion procedure with patient-specific lamina fit-and-lock templates for the thoracic spine: clinical article. J Neurosurg Spine. 2013; 19(2):185–90. [PubMed: 23705628]

76. Dickinson KJ, Matsumoto J, Cassivi SD, et al. Individualizing Management of Complex Esophageal Pathology Using Three-Dimensional Printed Models. Ann Thorac Surg. 2015; 100(2):692–7. [PubMed: 26234839]
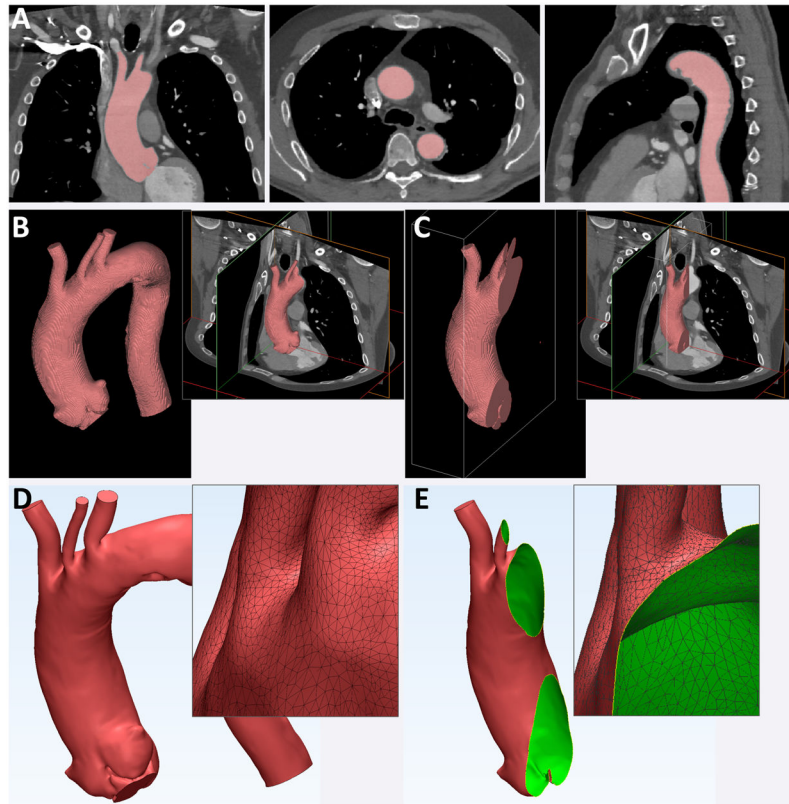
Figure 1. Generation of a 3D-printable STL model from a volumetric medical image dataset
The aorta and aortic arch vessels are first segmented from a contrast enhanced CT (A). The segmented image voxels identify the region of space occupied by blood and conversely this region of space is entirely filled by the individually-segmented voxels (B). If one were to cut through this region, it would simply expose the inner voxels that have been segmented (C). An STL model that can be 3D-printed is instead a surface composed of small triangles that encloses the segmented voxels (D; shown in red, with individual triangle outlines shown in inset). Cutting this surface merely exposes the inner side of the triangles (E; shown in green, with individual triangle outlines shown in inset).
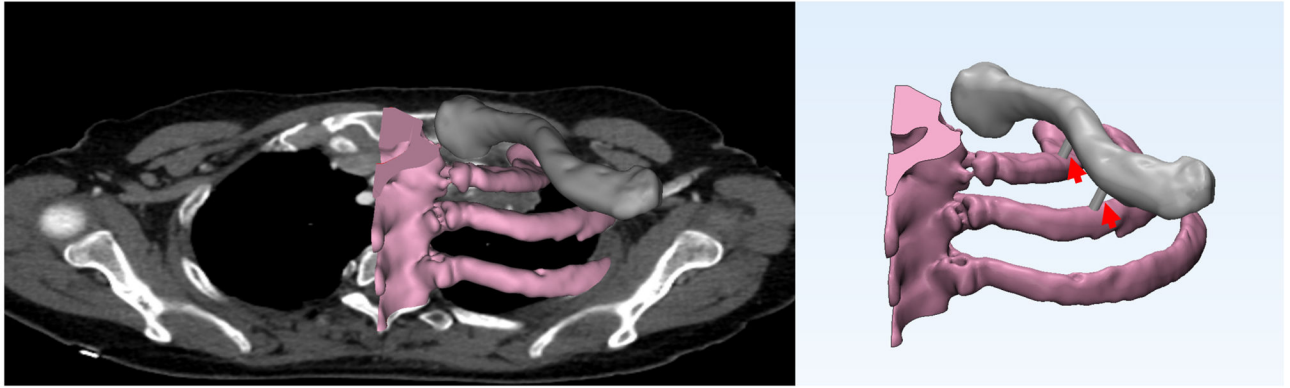
Figure 2. Addition of non-anatomic features to STL models of the clavicle and ribs segmented from a CT for inclusion in a superior sulcus tumor model

The model does not include the sternum to simplify interpretation by the surgical team. To maintain the relative position of the clavicle to the rib, two cylindrical connectors are added between the rib and clavicle STLs using CAD tools (red arrows). After printing, the two structures will stay united in one piece.
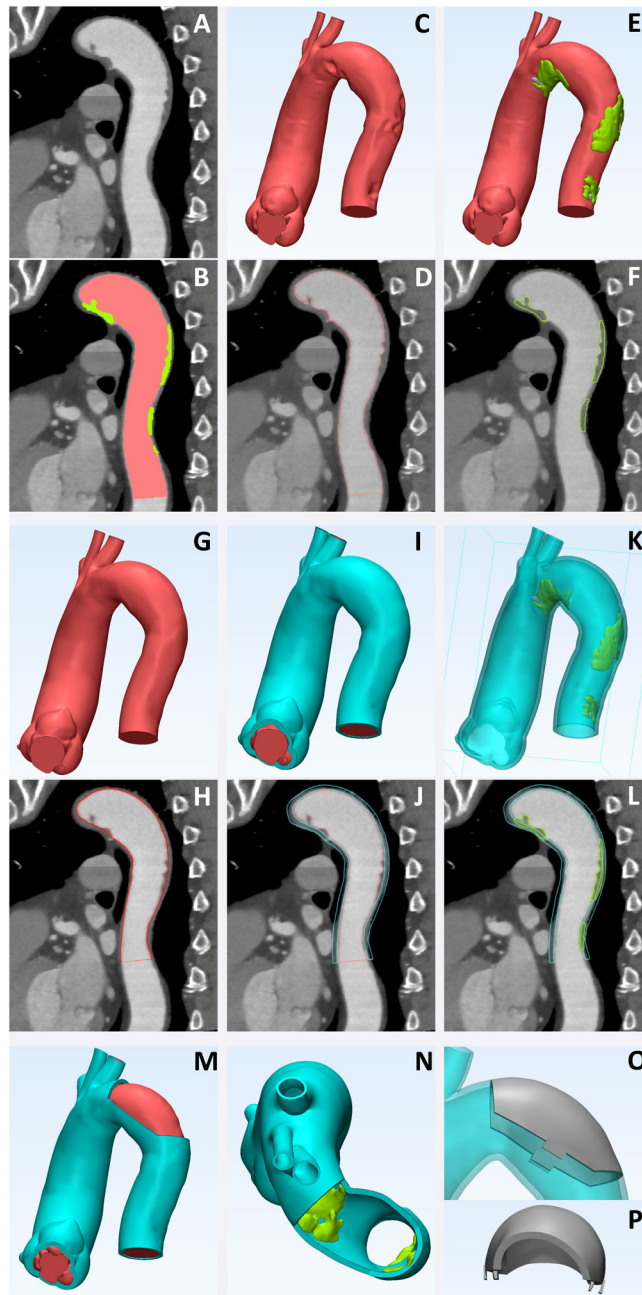
Figure 3. Complete sequence of STL generation and CAD manipulations to produce a model for planning of an endovascular procedure in an aorta with mural thrombi from contrast-enhanced CTA

CTA sagittal plane illustrates the contrast-enhanced lumen and thrombi (**A**). Segmentation of the blood pool and thrombus (**B;** lumen in red, thrombus in green) yields the corresponding STLs (**C,E**). The STL surfaces can be viewed superposed on the original CTA (**D,F**). These STL files can be printed but would not allow appreciating the extent of thrombus volume and lumen loss that are important for planning the procedure. An ideal 3D-printed model would show a hollow lumen with the thrombi extruding into it. This is achieved by first using "wrapping" and "smoothing" CAD manipulations on the blood pool STL to produce

the hypothetical ideal, smooth lumen (**G,H**; hypothetical lumen STL superposed on CT in bold red, and initial blood pool STL in lighter red). From this ideal lumen, a "hollow" procedure is applied to extrude a virtual vessel wall outwards from the lumen (**I,J**; virtual wall in turquoise). The mural thrombi now extend from the wall into the hollow lumen (**K,L**) as intended. A final CAD manipulation is used to create a cutout window in the vessel wall (**M**) to allow inspection of the lumen (**N**). The cutout portion is further augmented with snap-fit connectors using CAD tools to allow attachment to the main model **(O,P).** Same case as shown in Figure 1; the final 3D-printed model is shown in Figure 11.
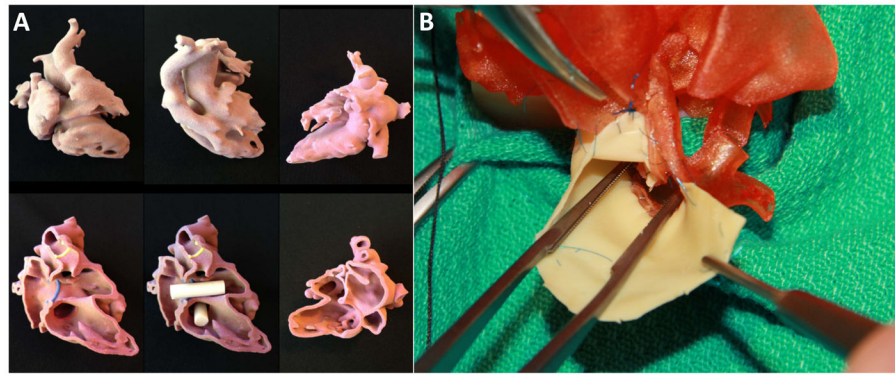
Figure 4. Congenital heart disease models for surgical simulation
Panel A depicts 3D printed model of a case of criss-cross heart with double outlet right ventricle. Upper row, shows the printout of the blood pool. Lower row shows a hollow model of the same case with a fictitious wall around the contrast-enhanced blood pool representing an approximation of the vessels and myocardium wall. Panel B shows a 3D printed model of a hypoplastic left ventricle heart syndrome during mockup operation for training and simulation of the Norwood operation. Figure courtesy of Prof. Shi-Joon Yoo from The Hospital for Sick Children, University of Toronto, Toronto, Canada.
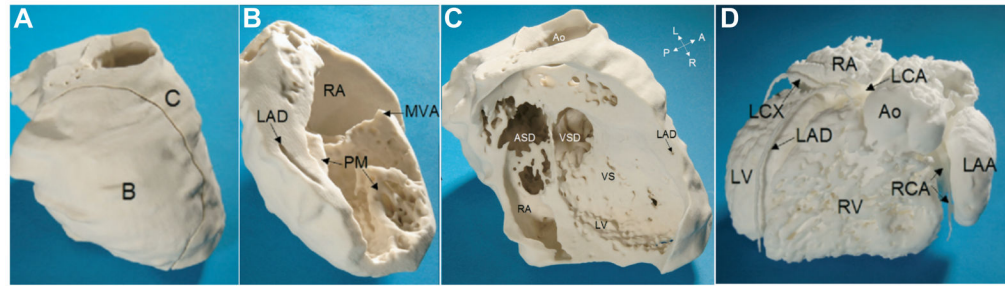
Figure 5. MRI-derived physical model of complex CHD

The 3D printed model of the myocardium plus vessel walls (Panel A) consists of two pieces (Panels B and C). A single cut divides the right atrium (RA) and the left ventricle (LV), allowing the view on the mitral valve annulus (MVA), two papillary muscles (PM), the left anterior descending coronary artery (LAD), ventricular septal defect (VSD), ventricular septum (VS), atrial septal defect (ASD), and the aorta (Ao). Panel D shows a 3D-printed model of the intracardiac volumes (blood pool) from the left anterior view. There is atrioventricular discordance with connections of the right atrium (RA) to the morphologically left ventricle (LV) on the right side. The left atrium (LA) with an enlarged left atrial appendage (LAA) is connected with the morphologically right ventricle (RV) on the left side. A dilated aorta (Ao) rises from the right ventricle. The left coronary artery (LCA) and right coronary artery (RCA) rise from a common origin of the coronary arteries (CO). (LAD = left anterior descending coronary artery; LCX = left circumflex; RV = right ventricle, A= anterior; L = left; P = posterior; R = right.) Reprinted with permission from reference [5].

Figure 6. 3D printing of complementary models for vascular pathologies
Representative example of a renal aneurysm contrast-enhanced CTA (A) used to produce 3D-printed models of the blood pool (B) and lumen for the left renal artery aneurysm (C). After examining the models, the surgeons opted for open repair of the aneurysm and patch angioplasty.

Figure 7. Models for planning and simulation of stent deployment for Mustard baffle revision in 45 year old male with history of complete transposition of great vessels

Panel A: Delayed venous phase CT demonstrating a large defect between the IVC and the pulmonary venous pathways at the rightward aspect of the baffle, a smaller defect between the SVC and the pulmonary venous pathways, and an intermediate-sized defect between the baffle and the right atrial appendage (red arrows). **Panel B:** 3D-printed model of the baffle designed as a fictitious wall around the blood pool (printed in gray) and including the ventricles (printed in white) for spatial orientation in this difficult case. **Panel C:** Removable ventricles and cut-out window of the wall of the pulmonary venous pathway/right atrium demonstrate the superior small and inferior large baffle defect (red arrows) and cut-out window of the right atrial wall demonstrates the third baffle defect communicating with the right atrial appendage. **Panel D:** A segment of the baffle was also printed in flexible material and used to simulate stent graft deployment to ensure an adequate proximal sealing zone. PV: Pulmonary vein, SVC: Superior vena cava, IVC: Inferior vena cava, RA: Right atrium, RV: Right ventricle, LV: left ventricle, RAA: Right atrial appendage.
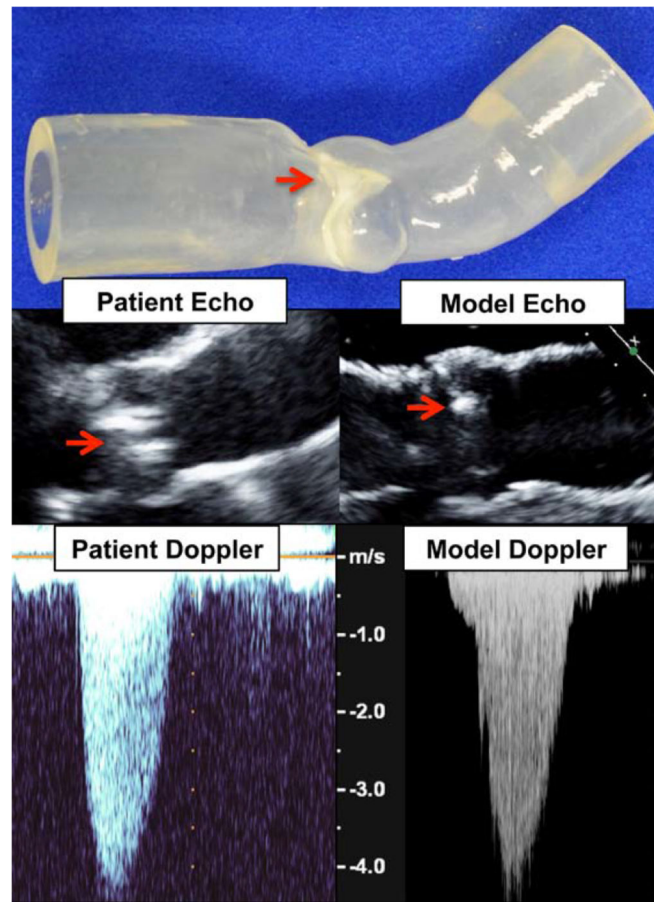
Figure 8. 3D printing of stenotic aortic valve for functional modeling
Top panel: clear model designed from patient CT examination indicates the location of a calcified aortic valve leaflet. Middle panel: Similar 2D echocardiographic image quality between patient and model with clear depiction of aortic root geometry and aortic valve leaflet calcification (red arrow). Bottom panel: Continuous wave Doppler imaging (matched to stroke volume and pressure gradient) demonstrates similar peak velocity, ejection time, and overall Doppler signal quality for patient and 3D printed model. Reprinted with permission from reference [55].
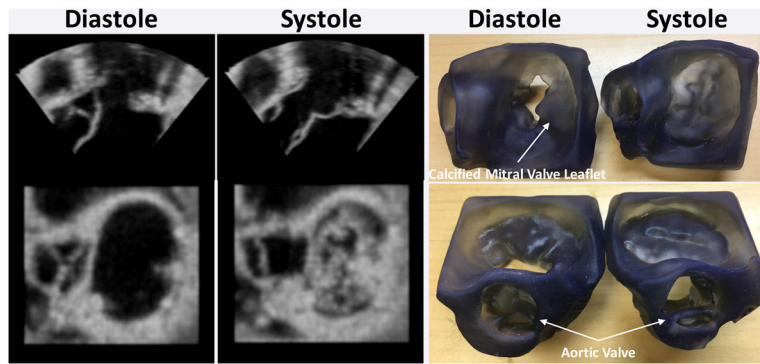
Figure 9. 3D printing of mitral and aortic valves from 3D TEE
Valves 3D printed in end-diastole and end-systole from lightly smoothed 3D TEE images to reduce speckles. Although the static models cannot assist in appreciating valve function, they clearly demonstrate the calcified middle posterior mitral valve leaflet impeding flow into the left ventricle. The models can thus be used to appreciate geometry and perform accurate measurements.
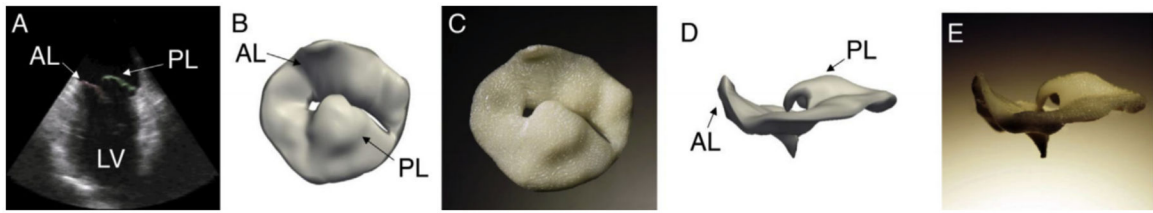
Figure 10. Three-dimensional echocardiography, virtual, and physical models of a patient with severe mitral regurgitation and a flail P2 leaflet segment

Long-axis view of the left ventricle (LV) and atrium during systole (A). The relative positions of the anterior (AL) and posterior (PL) mitral valve leaflets are indicated. Virtual (B) and printed model (C) viewed from the atrium. Virtual (D) and printed model (E) as viewed in profile from anterior to posterior commissure. Reprinted with permission from reference [61].
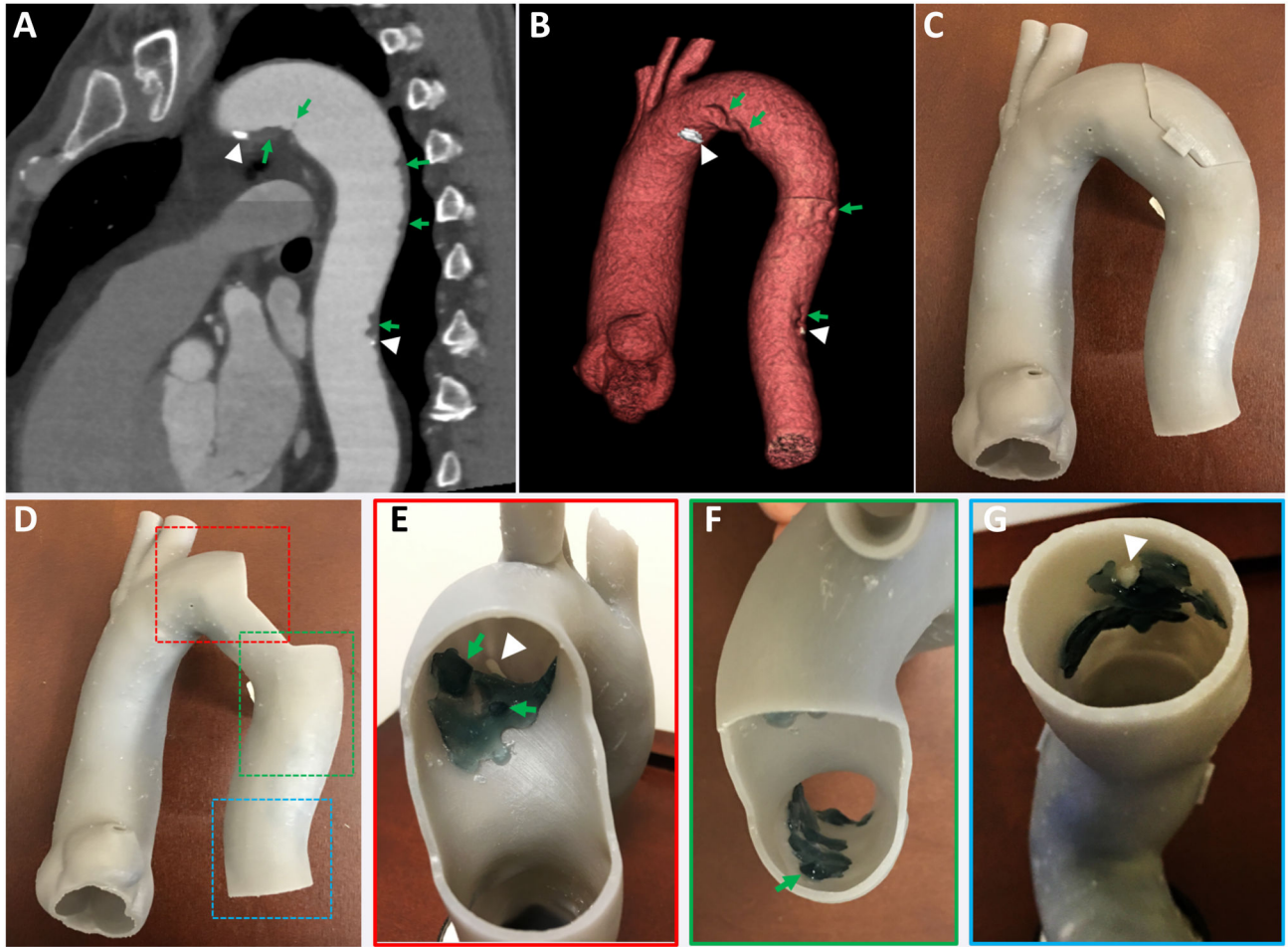
Figure 11. Model of aortic wall with mobile mural thrombi generated from CTA
The contrast-enhanced aorta with the mural thrombi seen as filling defects (A, green arrows) and high-density calcifications (A, white arrowheads). 3D volume rendering of the CTA conveys the locations of the calcifications and thrombi (B). A printed model of the aortic wall seen from the exterior (C) includes a cutout window that can be removed to inspect the aortic lumen (D). Inspection of the model from the cutout window (E,F) and viewed upwards from the descending aorta (G) allows appreciation of the location and size of the calcifications and thrombi (E-G, white arrowheads and green arrows, respectively) including with relation to the aortic arch vessels for planning of the percutaneous intervention.
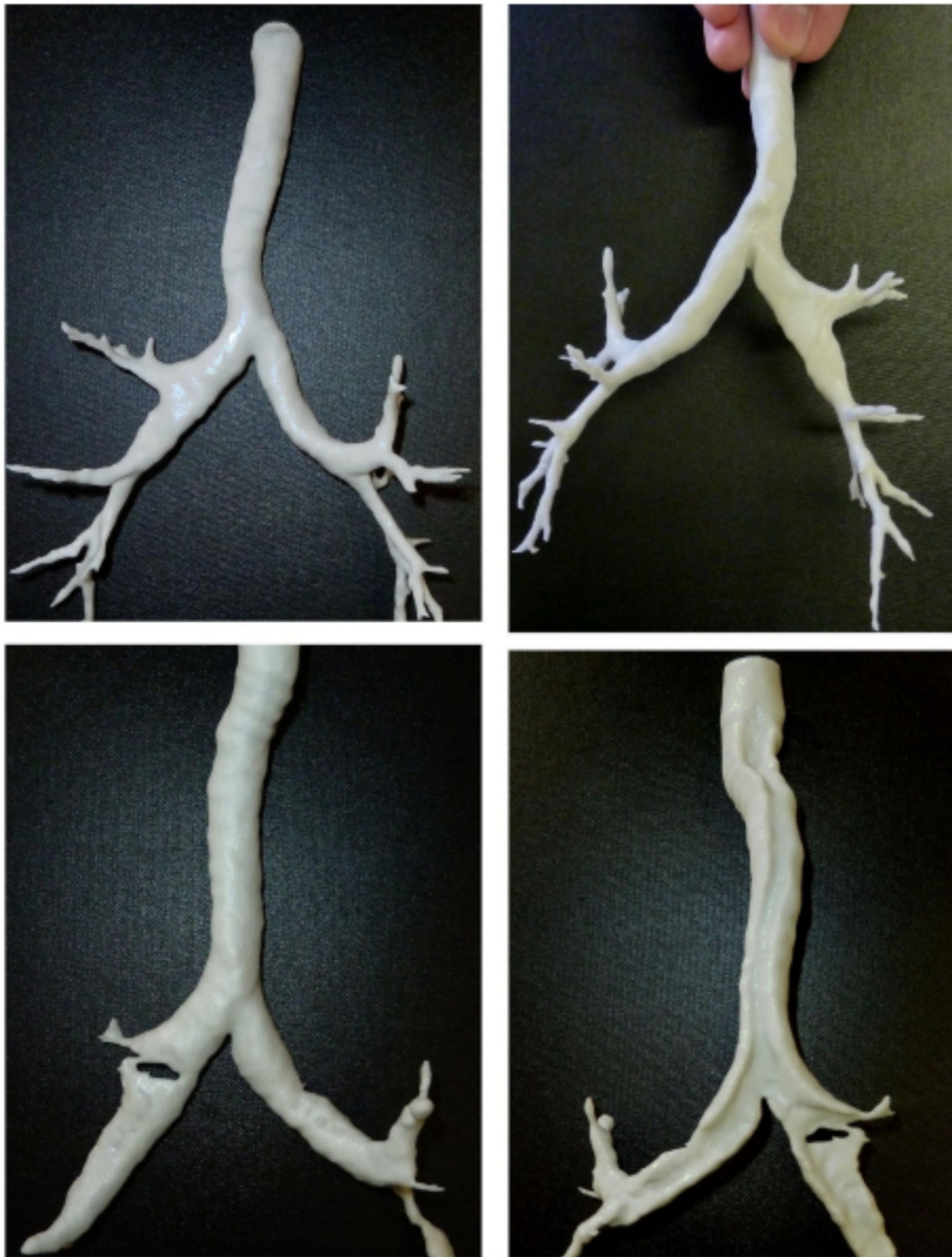
Figure 12. Models of the tracheobronchial tree of a 67 year old man with known relapsing polychondritis

Top row: anterior and posterior views of the inspiratory phase; bottom row: anterior and posterior views in expiration, evidently showing the collapsed airways. Reprinted with permission from reference [8].
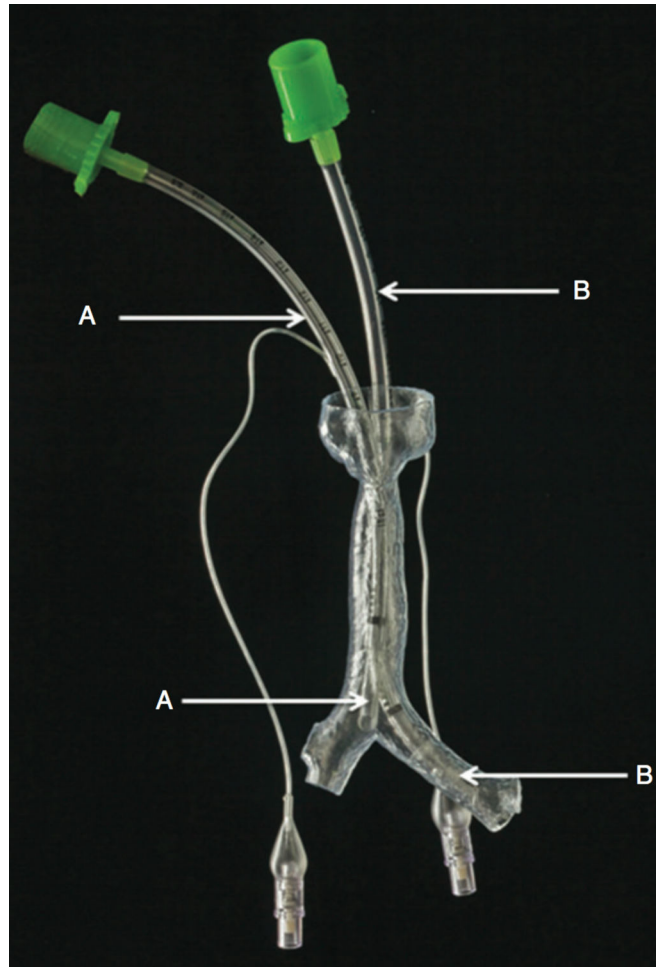
Figure 13. Airway model for planning of single-lung ventilation in a small child
The model allowed experimentation with various sizes of tracheal tube. In this example a size 3.5 Microcuff® tube was used, with cuff placed in the trachea (A) and with its tip at the carina, as well as a size 4 Microcuff® tube (B), with cuff placed in the left main bronchus. Reprinted with permission from reference [71].
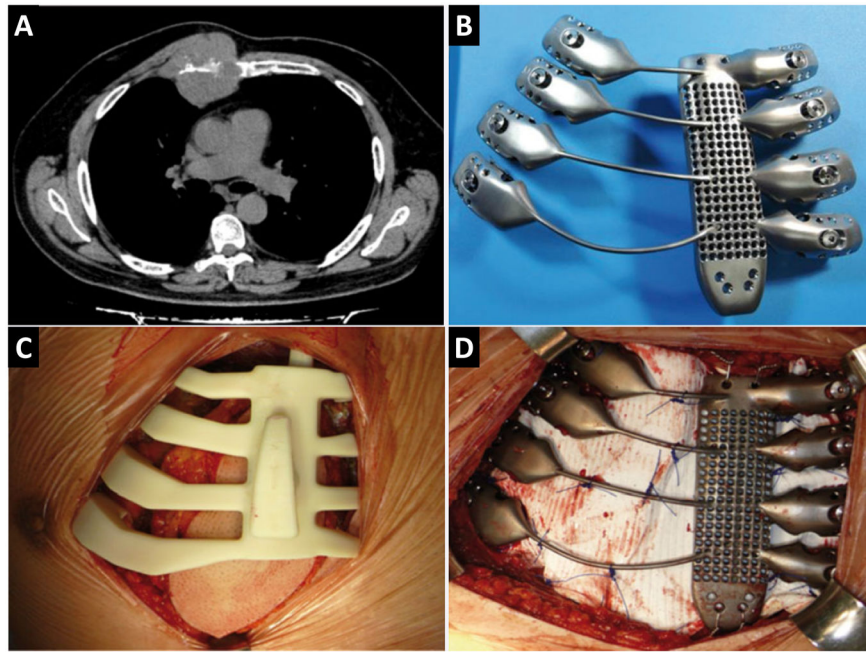
Figure 14. 3D-Printed custom-made titanium prosthesis for sternocostal reconstruction
CT scan showing involvement of chest wall structures (A). Final 3D printed implant design (B). A rigid template to allow precise setting of resection margins 3D-printed from biocompatible material is placed in the operative field (C) and final placement of the prosthesis with a Dualmesh® patch fixed to its rear side (D). Reprinted with permission from reference [16].
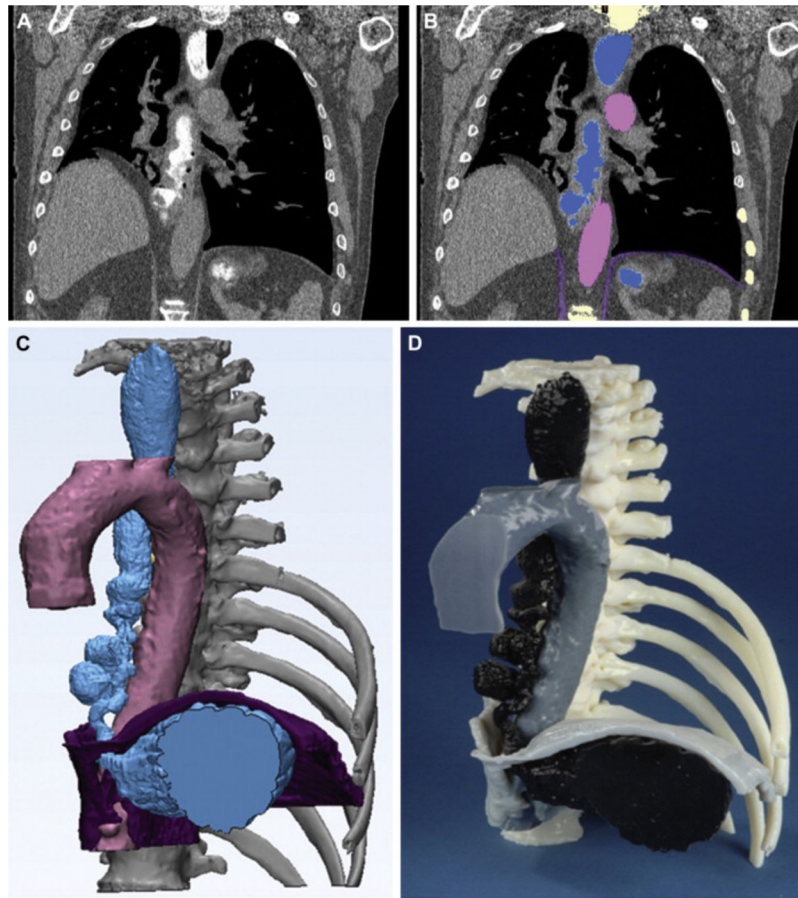
Figure 15. 3D printing of esophageal pathology
Patient with multiple esophageal diverticula imaged using a novel positive oral contrast and air technique to delineate the esophagus (A). The esophagus, stomach, diaphragmatic crus, aorta, and spine are individually segmented (B; each structure shown in different color). STL models of each segmented structure (C) are then 3D-printed in a multi-material, multi-colored model was printed (D). Reprinted with permission from reference [76].
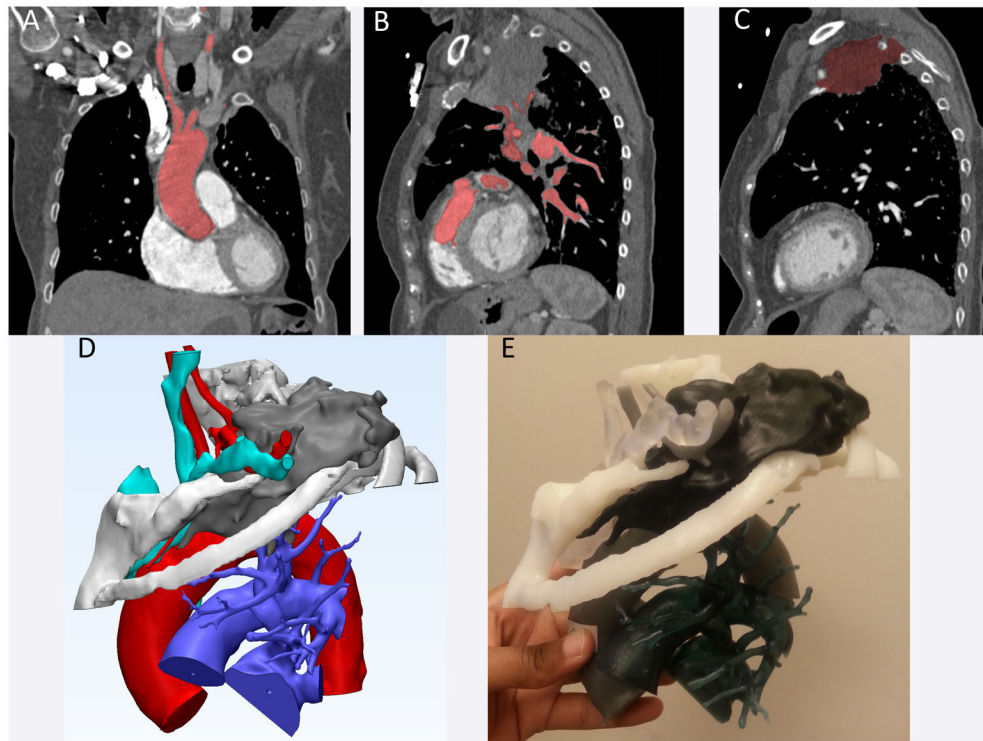
Figure 16. Model of a superior sulcus tumor

Contrast enhanced CT demonstrating the segmentation of the aorta in a coronal plane (A), and the pulmonary vasculature (B) and apical lung mass (C) in a sagittal plane. The complete STL (D) and 3D-printed models (E) include the mass, left 1st-4th ribs and upper thoracic vertebrae, thoracic aorta and great vessels, central and left upper lobe pulmonary vasculature, left subclavian and bilateral brachiocephalic veins, and the superior vena cava.
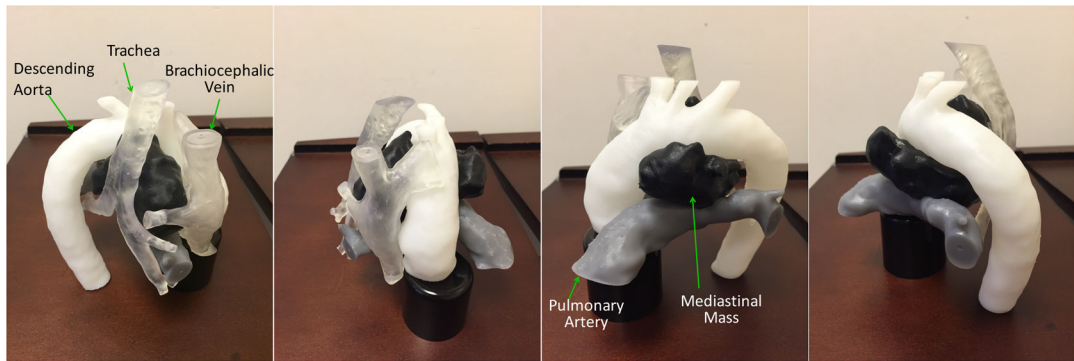
Figure 17. Model of middle mediastinal mass
Model includes the aorta, pulmonary artery, superior vena cava, and tracheobronchial tree, demonstrating a lobulated middle mediastinal mass extending from right paratracheal region to the aortopulmonary window and insinuating between the aorta and the main pulmonary artery.

Table 1

Summary of imaging modalities and protocols reported for cardiothoracic 3D Printing.

	Imaging Modality	Imaging Technique	Slice thickness (mm)
Congenital Heart Disease	*CT*	• ECG-gated breath- held contrast-enhanced, arterial plus delayed phase	0.5–1.25
	MR	• MRA with Gd-DTPA (fast low angle shot or steady state free precession) • ECG-gated respiration-navigated MRA with Ablavar® (blood pool contrast agent)	<1.5
Cardiac valves	*CT*	• Retrospective ECG- gated breath-held contrast-enhanced	0.5–1.25
	Echocardiography	• 2D/3D trans- esophageal echo • 3D trans-thoracic echo	N/A
Vasculature	*MR*	• MRA with Gd-DTPA • 3D T2 weighted black- blood fast spin echo	1
	CT	• Non-ECG gated Contrast-enhanced CT angiography	0.5–1.25
Tracheobronchial Tree	*CT*	• Contrast-enhanced CT in end-inspiratory and non-contrast dynamic CT in expiratory phase	1
Spine and Chest Wall	*CT*	• Non-contrast enhanced CT	0.5–1
Lung and Mediastinum	*CT*	• Non-contrast plus non- ECG-gated contrast- enhanced CT	1–3
	MR	• T2 post-contrast • T1 & T2 3D Fast Spin Echo	1–3

CT: Computed tomography; MR: Magnetic resonance; ECG: Electrocardiogram; MRA: Magnetic resonance angiography; 2D: two-dimensional; 3D: three-dimensional; Gd-DTPA: gadolinium-diethylenetriamine